CFD model-based analysis and experimental assessment of key design parameters for an integrated unglazed metallic thermal collector façade

P. Elguezabal[a*], A. Lopez[b], J. M. Blanco[b], J. A. Chica[a]

[a] *TECNALIA Building Technologies Division, Astondo Bidea, Edificio 700, Parque tecnológico de Bizkaia 48160 - Derio (Bizkaia), Spain*

[b] *Department of Nuclear Engineering and Fluid Mechanics, School of Engineering, UPV/EHU, Plaza Ingeniero Torres Quevedo 1, 48013 Bilbao, Spain*

* Corresponding author. E-mail address: peru.elguezabal@tecnalia.com (P. Elguezabal)

Abstract

Active façade systems incorporating solar thermal collectors currently offer very promising energetic solutions. From among the available systems, a simple solution is the unglazed heat collector for potential integration in low-temperature applications. However, when adopting system definitions, the modification of some design parameters and their impact has to be fully understood. In this study, the case of an unglazed collector integrated into a sandwich panel is assessed and a specific analysis is performed for a proper assessment of the influence of key design parameters. Based on that case study of the real built system, a CFD model is developed and validated and a parametric assessment is then performed, by altering the configurations of both the panel and the hydraulic circuit. In this way, the potential of each measure to harness solar energy can be evaluated and each parameter with its different level of impact can be highlighted, to identify those of higher relevance. A characterization of the real solution completes the study, by providing the efficiency curves and the total energy collected during the experimental campaign. The maximum estimate of the efficiency of a 6 m^2 façade was within a range between 0.47 – 0.34 and the heat loss factor was between 4.8 – 7.5. The case study exercises reveal the real energy efficiency and solar production patterns. There was also an opportunity to consider significant improvements to increase the output of the active façade. The main conclusions concerned the different criteria that improved the definition of the system and greater comprehension of alternative designs that may be integrated in the underlying concept.

Keywords: Solar Façade; Active Envelopes; Sandwich Panels; Unglazed and Integrated Solar Collector; Solar Heating

1. Introduction

The building industry, a sector that still shows very poor performance in terms of energy efficiency, has recently sought several alternatives for improvements to the carbon footprint throughout the building use phase. Europe clearly describes this situation with ambitious targets of 15 – 65 kWh/m^2 for Nearly Zero Energy Buildings (NZEB) [1], although the average consumption of the building stock in 2013 was 201.05 kWh/m^2 of final energy [2]. Over forthcoming years, the development of new and modern buildings equipped with the latest technologies should contribute to a reduction in that gap. However, the renovation sector is fundamental to balance the situation, because the rate of building stock renovation is still limited. Approximately 60% of current building stocks are likely to remain in use by 2050 in the European Union, United States, and Russia [3].

Very significant systems and promising technologies have been developed over the past few years and continue to be, as the momentum of the sustainable and renewable technologies gathers pace in the industry and thank to a continuous R&D effort. A first step will be to reduce consumption by minimizing demand. In a second step, the reduction in energy requirements will mainly be met through Renewable Energy Sources (RES) and preferably from onsite production. Finally, with the minimization of energy requirements and the incorporation of the RES contribution, some necessities might not be covered by intermittent renewable production. A third step will therefore be to improve the response of the whole system dealing with smart and efficient management of the main energy sources and components in the system.

The façade functions in this scenario as the interface connecting the interior where comfort is a priority and the exterior under variable environmental conditions. Renewable energy is unlimited and accessible, and the envelope should be able to harness those sources, becoming more than a simple barrier for energy losses.

1.1 Integrated solar collectors as active façades

The definition of the “active” façade behavior differs depending on the source that is consulted. Some authors [4 - 11] have examined the capacity of capturing renewable energy on the façade. Others [12 - 13] mention higher dynamism and movable parts that define more “adaptive” façades, usually with more than an active response and generally combining energetic integration with additional features, in terms of solar protection, shape modification, and automated components that alter the external shape and appearance of the skin.

The concept of interest to the present study has been variously defined as Solar Façade (SF), Active Solar Thermal Façade (ASTF), and Building Integrated Solar Thermal Systems (BISTS) [14 - 15]. These systems integrate the collector technology in the building envelope, with the twin function of protecting the interior from the exterior, together with a solar thermal energy collector device.

A standard classification of solar thermal collectors found in stationary applications would list compound parabolic collectors, vacuum tube collectors (evacuated pipe collectors), flat-plate glazed collectors (generally shortened to flat-plate) and unglazed collectors (a variation of the flat-plate model). A classification into three categories also refers to the temperature levels that differ in each solution [16]. Working temperatures are significantly lower for unglazed panels (25-50 ºC) compared with flat-plate collectors (50-100 ºC) and vacuum collectors (100-140 ºC) [17].

A key component is the absorber [18], generally manufactured in dark colors to maximize absorption [19]. Their materials are metals or UV resistant polymeric materials, although copper, aluminum, and steel are used for absorbers in flat-plate and vacuum-pipe systems. The use of less conductive materials is less significant in flat plate systems, although some alternatives are also feasible for unglazed collectors, aiming for more economic solutions. Polymeric, [20 - 21], Concrete [22 - 23] and Ceramic [24 - 25] absorbers have been proposed as cheaper alternatives, as well as solutions combining different materials [26 - 27].

Finally, there are two possible thermal fluids for heat transfer; liquid (water and water mixtures) and air. Liquid-based applications are the most common ones [28], probably because of the higher density and specific heat that influences efficiency, however some interesting applications with air-based transpired solar collectors, have been used for façade integration [29 - 30].

The use of solar thermal collectors worldwide is quite extensive [28], among which evacuated panels are the most widely installed (72%), mainly in response to growing demand in China. Flat-plate collectors are the first option in Europe (22% worldwide) and unglazed collectors (6% worldwide) in the USA and Canada. Mainly used for DHW production, especially for flat plate and evacuated systems, unglazed collectors are usually associated with swimming pool water heating devices. Combi systems in Europe for both Domestic Hot Water (DHW) and space heating are worth mentioning.

Unfortunately, exhaustive information is unavailable to estimate the number of active solar thermal façades that are currently installed, as well as their typologies and potential efficiencies. There are some reviews of possible solar façade applications in the literature [7, 9 - 10, 31 - 33]. Interest in such solutions to contribute to the production of energy for heating, cooling and DHW purposes has likewise been assessed [34]. Although some standardization for BISTS is suggested [35] the level of application of solar façades is yet to become a widely implemented standard solution.

The incorporation in a façade of all these concepts for it to become an active element is a marked tendency nowadays and an ongoing process with several research initiatives developing ASTFs. The positioning of collectors on vertical planes of a building envelope also implies a lower incident irradiation than horizontal or optimum tilt [36]. However, if a south-facing wall is chosen, irradiance will remain quite regular and stable with no overheating throughout the whole year [17].

There is a significant variety of technologies for ASTFs with different degrees of sophistication [37]. New developments have been presented over the past years [38,39,41-43], however, the presence of these solutions is still largely testimonial [44], due to inadequate knowledge and resistance to change in the sector, even more so for technological solutions directly identified as very costly.

The unglazed panel simplifies the solution by leaving the absorber on the outer face of the panel that achieves a higher level of integration [6]. These represent simpler and less technological systems, but also significantly lower investment [45] and they are of special interest to the renovation sector. But when approaching a design process involving a solar façade with an unglazed collector, the impact of modifying some design parameters is not so clear.

The review of the current state of the art reveals quite a large quantity of polymeric systems for the “swimming pool” application. When looking at ASTFs and specifically at those with metallic absorbers, the number of available systems for unglazed and low temperature systems is of less significance. Remarkable systems are the concepts provided by Énergie Solaire [46], Solabs [47 - 48], Triple Solar [49], WAF [7], BATISOL, [50] and InRoof [51].

1.2 Novel unglazed solar collector integrated into a metallic sandwich-panel façade

The present study is focused on the behavior of a low temperature active façade composed of an unglazed collector and a steel sandwich panel. The system was developed as part of a research project (BASSE) [52] concluded in 2016, where the design of an innovative solar panel and its interconnection to a heat pump was developed.

The application of sandwich panels in industrial and commercial buildings is extensive thanks to a very competitive cost/performance ratio. However, their use in offices and especially in the residential sector is still quite unusual. The purpose of the BASSE project was to exploit the high conductivity of steel, by activating the passive behavior of the sandwich panel, turning it into a low temperature solar collector on an active envelope. Alternatives to the current sandwich panel, clearly designed for industrialization and high-scale production, were actively pursued.

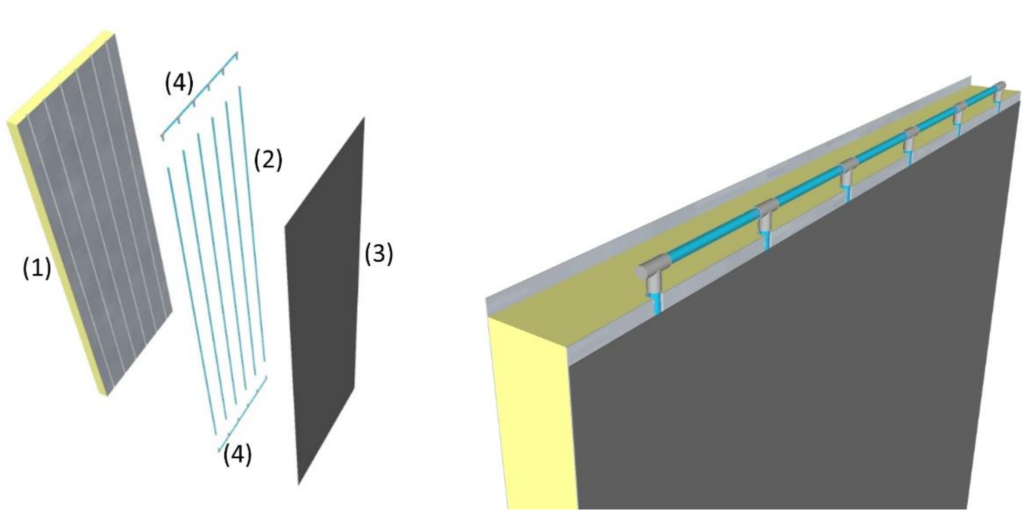

Figure1: Sandwich panel integrating an unglazed solar collector. Main components of the solution (left) and detail of the top side for the assembled panel (right).

The resulting design of this initial solution as an ASTF consisted of four main components. The sandwich panel with a polyurethane insulated core (1) combined with two slotted steel skins. Plastic pipes (2) installed in the slots of the external skin for completion with the final steel cover (3) functioning as a solar absorber. Each panel has 6 parallel tubes and modular header fittings for their interconnection (4) also provided inside the module. Dimensions of the standard panel are 3 m long, 1 m wide and 0.8 m thick. A complete system was installed in a real building [53] and the tests demonstrated the potential of such solutions for significant reductions in the final consumption of energy.

2. Aims and Methodology

The object of the study is the analysis of the unglazed collector, as part of the active façade, evaluating possible design alternatives by means of a parametric study. Based on the design described in Figure 1, the analysis examines the performance of the ASTF in depth, in continuance of the research activity initiated in the BASSE project. To do so, an initial review of theoretical models in the literature will be performed. The conclusions of this review will then set out the definition of a Computer Fluid Dynamic (CFD) model for implementation. The next step will be to validate the model using real measured data taken from a real active façade. With the validated model, a parametric study will be developed using reference values based on the main technologies and materials available to solve the system. Finally, the energy output of the real solution and its performance will be estimated and characterized using the data measured under real working conditions.

3. System modelling

3.1 Theoretical model

Efficiency is the main parameter that characterizes the behavior of a thermal collector. It will also be the main criteria for evaluating the different alternatives for the system. As indicated in equation 1 [54], efficiency is a relation between the useful energy and the incident solar energy. The energy output is defined as well as a function of the temperature difference between the inlet and outlet of the fluid through the collector (equation 2).

$$h = \frac{Q}{A_c\, I_{sol}} \tag{1}$$

$$Q = \dot{m}\, C_w\, (T_{out} - T_{in}) \tag{2}$$

A commonly used expression to describe the efficiency of collectors is described in equation 3 as a function of absorptivity (α), the collector heat removal factor (F_R), and the heat transfer coefficient (U_L):

$$h = F_R\, a - F_R\, U_L \frac{(T_{in} - T_{amb})}{I_{sol}} \tag{3}$$

where, F_R and U_L will usually represent the experimental test results. Reference values taken from some commercial systems of the ranges that unglazed collectors will usually have in terms of (F_R α) and (F_R U_L) are included in Table 1. It is worth noting that all the parameters indicated in Table 1 are calculated for wind speeds in the range of 0 – 3 m/s and for panels with an area less than 2.3m^2.

Table 1: Efficiency parameters for different unglazed solar collectors

System	$F_R\, a$	$F_R\, U_L$
Aluminum Absorber (InRoof.Solar) [55]	0.42 – 0.6	9.74 – 13.44
Stainless Steel Absorber (AS Energie Solaire) [56]	0.86 – 0.92	11.26 – 18.61
Copper Absorber (TECU® Solar) [57]	0.59 – 0.8	9.05 – 12.26
Titanium zinc Absorber (QUICK STEP®) [58]	0.5 – 0.54	12.87 – 14.78
Aluminum Absorber – System 1 [59]	0.55 – 0.58	7.44 – 14.0
Aluminum Absorber – System 2 [59]	0.83 – 0.89	12.7 – 19.7

In addition, some analytical calculations are also available [54] for determining F_R in a tube-and-sheet configuration, while U_L can be estimated using the resistance equivalency for the effect of the energy losses due to the conduction, convection and radiation effects.

In the determination of F_R, additional factors such as the collector efficiency factor (F'), the standard fin efficiency for straight fins (F) and the C_L variable are required. F' and F are dimensionless while C_L represents m^{-1}. Likewise, F', F_R and U_L permit the calculation [54, 60] of fluid temperatures at the collector outlet (T_{out}) and the mean temperature in the absorber (T_s), as shown in equations (8) and (9), respectively.

$$F_R = \frac{\dot{m}\, C_w}{A_c\, U_L}\ [1 - e^{-\left(\frac{A_c\, U_L\, F'}{\dot{m}\, C_w}\right)}] \tag{4}$$

$$F' = \left(\frac{W}{D_i + (W - D_i)\, F} + \frac{W\, U_L}{\pi\, D_i h_f}\right)^{-1} \tag{5}$$

$$F = \frac{\tanh[C_L(W - D_i)/2]}{C_L(W - D_i)/2} \tag{6}$$

$$C_L = \sqrt{\frac{U_L}{\lambda_s t_s}} \tag{7}$$

$$T_{out} = T_{amb} + \frac{\alpha I_{sol}}{U_L} + \left(T_{in} - T_{amb} + \frac{\alpha I_{sol}}{U_L}\right) e^{-\left(\frac{A_c\, U_L\, F'}{\dot{m}\, C_w}\right)} \tag{8}$$

$$T_s = T_{in} + \frac{Q}{A_c\, U_L\, F_R}(1 - F_R) \tag{9}$$

In the above-mentioned case, equations 4 to 9 are applied in a complex system of coupled non-linear equations that require multiple iterations for their solution. The dependency of some parameters on temperature also needs consideration and for the parametric study that is intended to be developed, it will require the use of specific calculation software.
The analytical approach of some authors [60] uses the above equations for a parametric assessment. However, the use of a CFD model provides wider flexibility to consider multiple alternatives including dynamic inputs for comprehension of the system and its evolution over time. The benefit of working with a previously built façade is an advantage, giving the opportunity to validate the model against the real system.

The CFD approach with experimental validation has also been applied to concrete unglazed collectors [61], copper absorber glazed collectors [62] and aluminum absorbers for unglazed collectors [63]. CFD without experimental validation is also described for aluminum sandwich panels [64] and for unglazed solar collectors [65].

3.2 CFD model definition

3.2.1 Physical model

A bespoke finite element model computed in ANSYS FLUENT® V18.2 was developed, based on the prototype of the active façade (Figure 1). The function of the model was heat transfer calculation within solids and between solids and fluid, which represent the two main thermal processes inside the collector. These effects including their symmetries on both sides are represented in Figure 2, as well as the closed air chamber on the back side of the sandwich panel where only natural convection is considered.

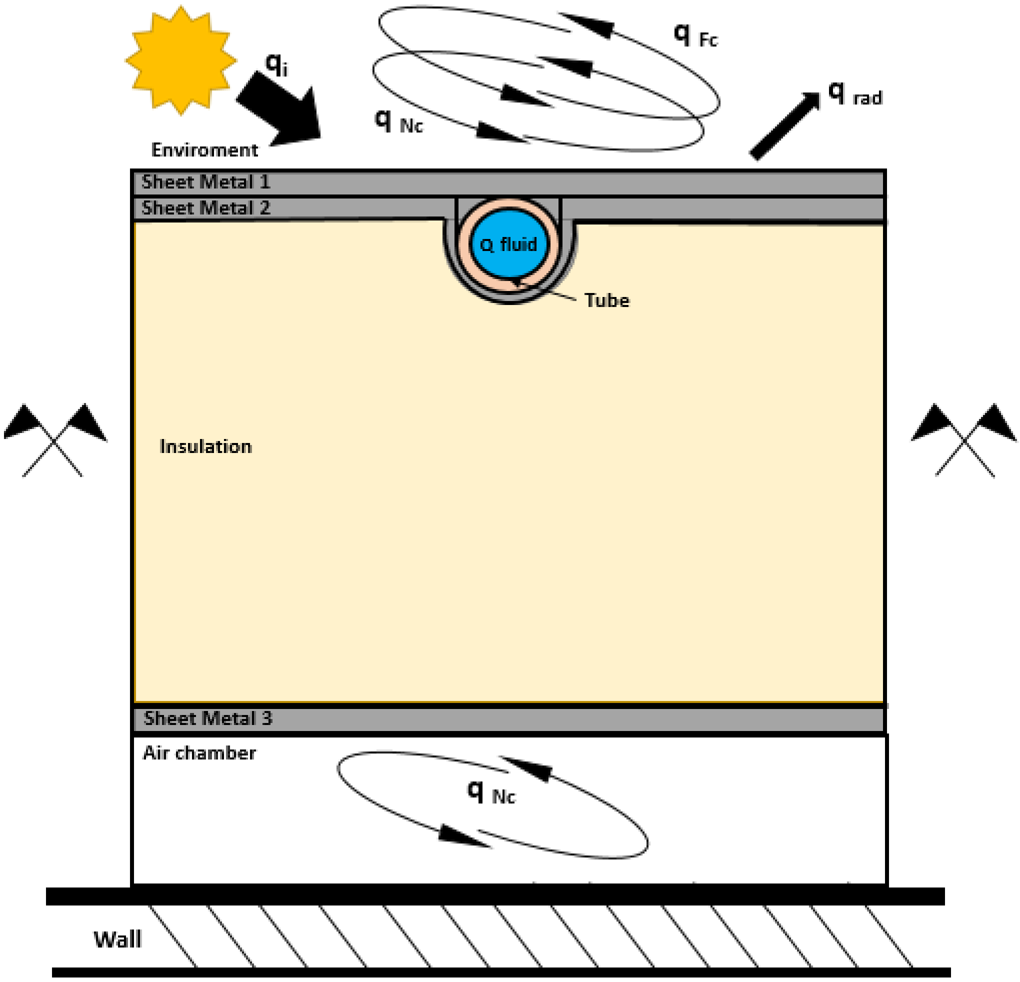

Figure 2: Main phenomena considered at domains

This analysis is subject to the following assumptions:

- The heat transfer coefficient between the fluid and the pipe is constant
- The back and edges of the collector are perfectly insulated
- There is perfect contact between the pipe and surrounding metal sheet and between the sheets

- The properties of the materials are independent of temperature

The main thermal phenomena under consideration are solar irradiation as the main energy source, surface radiation of the absorber back to the external air, natural convection to the air and forced convection because of the wind effect. Conduction between solids is calculated by means of the general energy equation and convection between the pipe wall and the fluid is also considered. As a result, the temperature gain of the fluid when passing through the pipe in the longitudinal axis will represent the performance of the collector and therefore the energy extracted.

For the incident radiation, (q_i), a "heat flux" was modelled [66], so the heat absorbed by the exposed surface of the collector is equal to solar irradiance and surface absorptance. The energy absorbed is obtained by the expression:

$$q_i = \alpha I_{sol} \tag{10}$$

The radiation emitted back (q_{rad}) by the external sheet to the air is the result of the emissivity and Stefan Boltzmann's constant as a function of the temperature difference of the steel sheet with the environment.

$$q_{rad} = \varepsilon\sigma\left(T_{sky}^4 - T_s^4\right) \tag{11}$$

$$q_{n,c} = h_{W,n}(T_{amb} - T_s) \tag{12}$$

$$q_{f,c} = h_{W,f}(T_{amb} - T_s) \tag{13}$$

Heat is also transferred back to the air by natural (equation 12) and forced convection (equation 13) [22]. A combined convective coefficient (h_w) is used, taking wind speed as the main criteria for the model that is under development. Different correlations were evaluated, based on the alternatives available in the bibliography, in order to select this h_w parameter [67]. In the validation of the model, three alternatives will be considered for wind speeds V_W < 5m/s, as described in equations (14) to (16)

$$h_W = 2.8 + 3V_W \qquad [68] \tag{14}$$

$$h_W = 5.7 + 3.8V_W \qquad [69] \tag{15}$$

$$h_W = 8.55 + 2.56V_W \qquad [70] \tag{16}$$

Thus, the overall heat released by the wall to the air is computed as mixed boundary condition combining convection and radiation [71]:

$$q = h_w(T_{amb} - T_s) + q_{rad} \tag{17}$$

Convection in the rear sheet to the air chamber is an effect that is exclusively considered for the assessment of the insulation material (Section 5.1), as this effect merely influences cases in which there is a small quantity of insulation. In the other cases, an adiabatic wall will be considered with negligible external surface interrelation where each zone can be calculated independently.

The convective heat transfer between the fluid zones and the corresponding faces are solved by coupling the momentum and energy equations. The SIMPLE method is used for the discretization of the pressure and second order upwind for momentum and energy equations.

The Prandtl number is given by equation (18), where C_p is specific heat, μ viscosity and λ_f thermal conductivity of the fluid. A 6.9 Prandtl number for water is considered.

$$Pr = \frac{C_p \mu}{\lambda_f} \tag{18}$$

The Reynolds number for the flow through the pipe is given by equation (19). Being V velocity of the fluid, D_i hydraulic diameter and $\mathcal{V}_k$ kinematic viscosity. The resulting Reynolds number (26485) represent a turbulent flow ($Re \geq 4000$).

$$Re = \frac{V * D_i}{\mathcal{V}_k} \tag{19}$$

Therefore, the k-ε standard turbulence model is used for the numerical description of the fluid behaviour. In this conditions Reynolds-averaged Navier-Stokes (RANS) equations can be considered.

For the energy equation, the conduction heat transfer governed by Fourier's law was considered. The heat flux absorbed by the internal fluid passing through the pipe, q_f, is described by equation:

$$q_f = h_f(T_f - T_p) \tag{20}$$

Simulated under steady state conditions, the model calculates the heat transfer effects that are described giving as results the outlet temperature (T_{out}) and the external sheet temperature (T_s). T_{out} will calculate the energy gained in the panel as the difference between the inlet and the outlet temperatures for a certain mass flow (equation 2). Combining equations 1 and 2, the solar collector's efficiency can be calculated by equation 21. Depending on the inputs, the instantaneous or mean daily efficiencies can be estimated.

$$\eta = \frac{\dot{m}\, C_w (T_{out} - T_{In})}{I_{sol} A_c} \tag{21}$$

3.2.2 Geometry and mesh definition

The scheme of a 3D geometry set-up that represents the main components of the collector is depicted in Figure 3. It has an interior and an exterior wall where the fluid passes through the model, as well as a mass flow inlet and a pressure outlet. All these parameters are indicated as boundary conditions for the different domains in Figure 3.

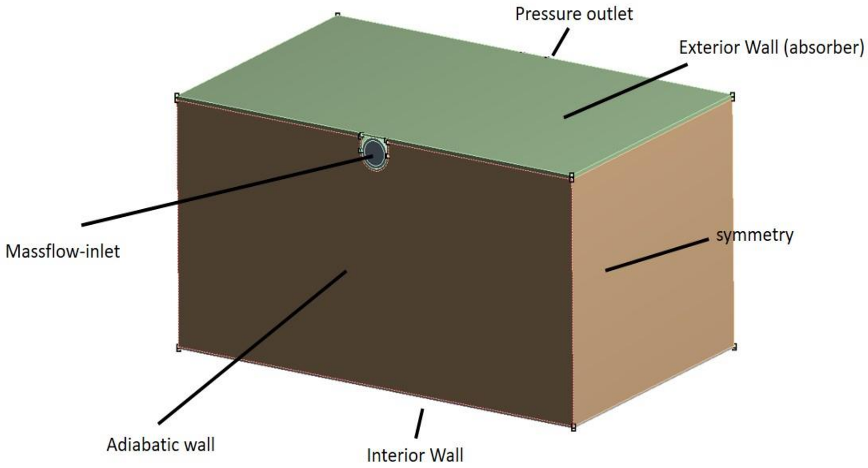

Figure 3. Boundary conditions at domains

The finite element mesh is generated using triangular and tetrahedral elements with a higher mesh density where heat exchange between bodies is more significant (Figure 4).

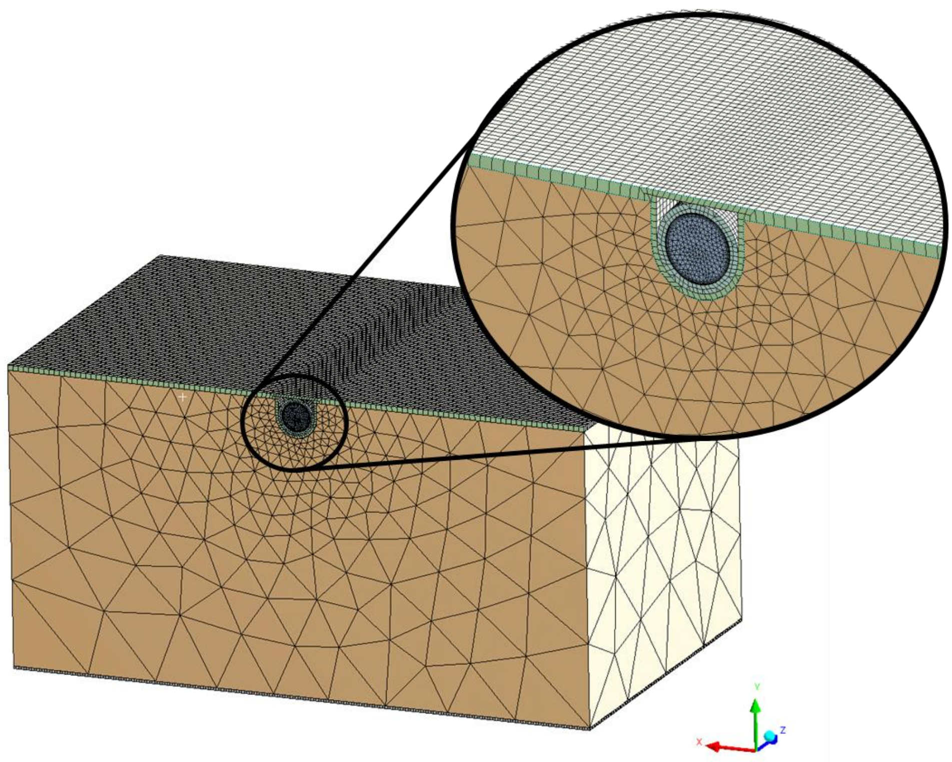

Figure 4: Detail of model meshing

A mesh sensitivity analysis was also performed using the real values measured during 18th of June 2017. Figure 5 shows the differences between measured and simulated results. Table 2 provides the Predicted Mean Absolute Error PMAE [72] for different meshes.

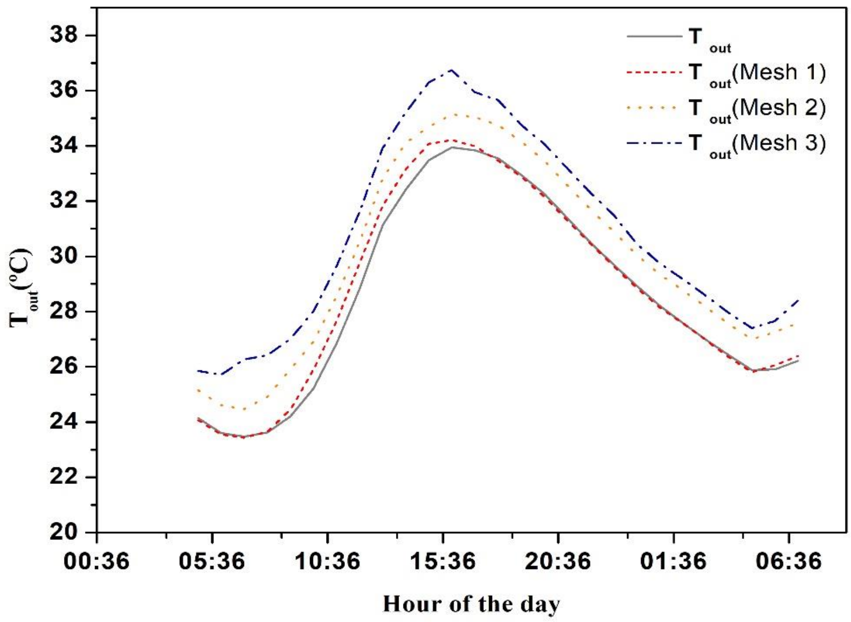

Figure 5: Calculated T_{out} results for three different meshes and PMAE for each case.

Table 2. PMAE for the mesh sensitivity analysis

Mesh (number of cells)	PMAE (%)
Mesh 1 (509,385)	0.81
Mesh 2 (361,407)	3.81
Mesh 3 (284,584)	7.17

3.2.3 Model upscaling

Due to the parallel configuration of the collector connected through a top and bottom header, the system can be simplified to a 100 mm long x 160mm wide section containing one single pipe. The headers provide a uniform flow to the pipes and represent a small area compared to the complete surface of the collector, so it can be ignored in the calculation [54]. The symmetry condition on the lateral faces permits the consideration of multiple pipes and consequently the width of the section will determine the distance between parallel pipes as represented in figure 6.

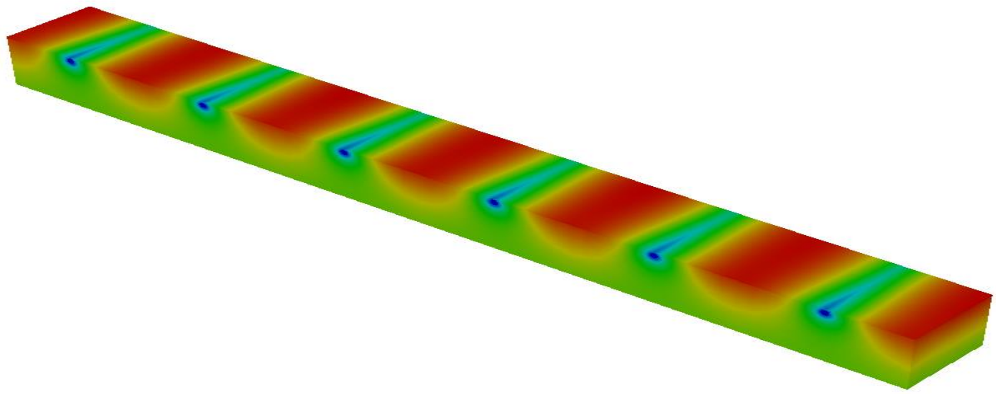

Figure 6. Representation of symmetry condition in the model to represent multiple parallel pipes

Additionally, longer sections can be considered and calculated by assuming the same hydraulic residence time (τ) for different pipes, enabling the calculation of the panel regardless of the length, as can be seen in Figure 7.

$$\tau_1 = \tau_2 \tag{22}$$

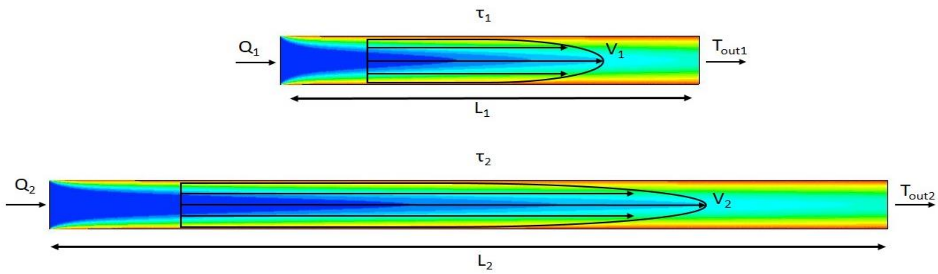

Figure 7: Representation of different pipe lengths for calculation with equivalent flow

Therefore, a hydraulic residence time is calculated for a target length according to equation (22). And by rearranging equations (22) to (24), with equal pipe sections from both pipes, an equivalent mass flow for the model can be calculated, as expressed in equation (25):

$$\tau = \frac{L}{V} \tag{23}$$

$$V = \frac{\dot{m}}{S} \tag{24}$$

$$\dot{m}_1 = \frac{L_1 \dot{m}_2}{L_2} \tag{25}$$

The consideration of both symmetry conditions on one axis and flow equivalency for a different panel length on the other axis permit the optimization of the model for quick computational calculation and tests the information that is required for the study.

4. Experimental validation

4.1 Test set up

In the demonstration phase of the BASSE project, the system was installed on the wall of Tecnalia's Kubik® experimental building [73] at Derio, Spain (1,300 kWh/m^2 mean annual horizontal irradiation). As part of that project, testing took place over 4 months in 2016. A total of 6 south-oriented active panels of 3m^2 each were fitted on the external façade of the Kubik building as shown in Figure 8.

As a progression over that initial campaign, an additional extensive experimental campaign was developed as part of current study during 2017. Specific days were selected from this second campaign for the validation phase. The main components of the solar loop will be considered, thus the other system components such as the heat pump, remain outside of the scope of study.

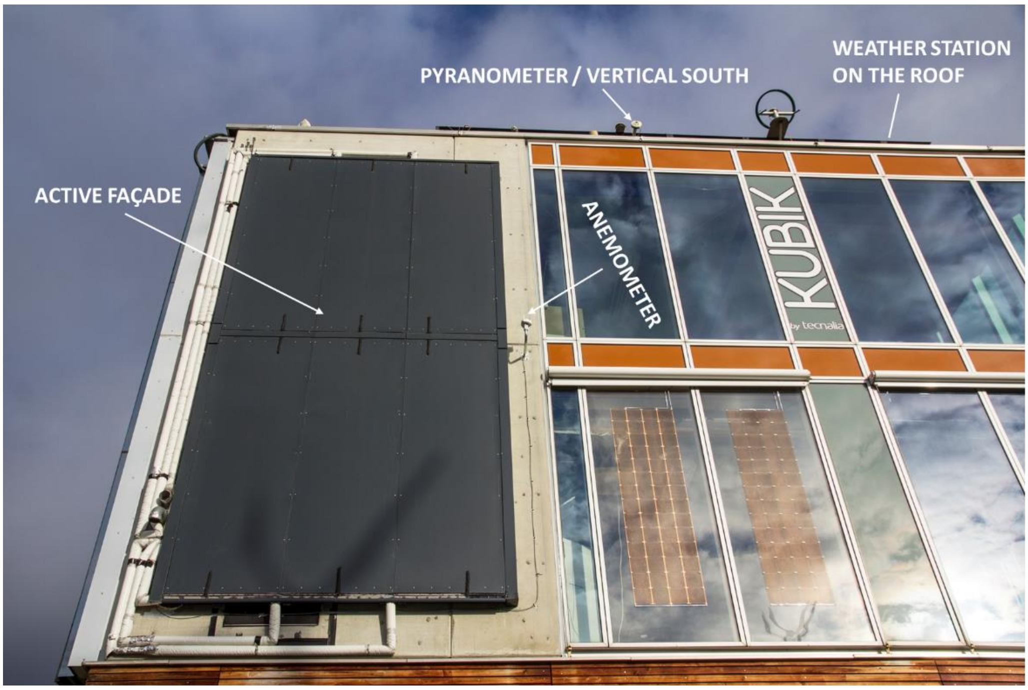

Figure 8: Panels installed in the south façade of Kubik® building

The main components of the solar loop are the active façade (6 panels), the storage tank (285L), the distribution system, the circulatory pump and the measurement devices. The description of the complete solar loop is provided in Figure 9. The configuration for the active façade was a set of 2 panels in series to configure 6m long batteries that were latter connected in parallel.

The measurement system is composed of different devices as represented in Table 3. A total of 12 temperature sensors are located on the surface of the panels to monitor the mean absorber plate temperature (T_s), 2 sensors in the storage tank and 4 sensors for the fluid temperature with a common input (T_{in}) and three output temperatures (T_{out}) coming from each battery. The flowmeter registers the mass flow ($\dot{m}$), the pyranometer (P) the irradiation (I_{sol}) on the vertical south orientation, a weather station on the roof monitors the external ambient temperature (T_{amb}), and the anemometer (A) records wind speeds (V_w) and wind direction.

Table 3. Experimental equipment's description

Parameter	**Measurement device**	**Type/Model**	**Uncertainty**
Surface temperature (ºC)	RTD – PT100	Thermo Sensor GmBH	±0.1 ºC
Fluid temperature in pipes and storage tank (ºC)	RTD – PT100	Thermo Sensor GmBH	±0.1 ºC
Mass flow (l/min)	Ultrasonic Flowmeter	Kamstrupp Ultraflow Multical 801	±0.0132 l/seg
Irradiation (W/m^2)	Pyranometer	Kipp & Zonen CMP – 6	± 5%
Wind speed (m/s)	Anemometer	Vaisala WXT520	± 3%
External ambient air temperature (ºC)	RTD – PT100	Vaisala WXT520	± 0.3 ºC

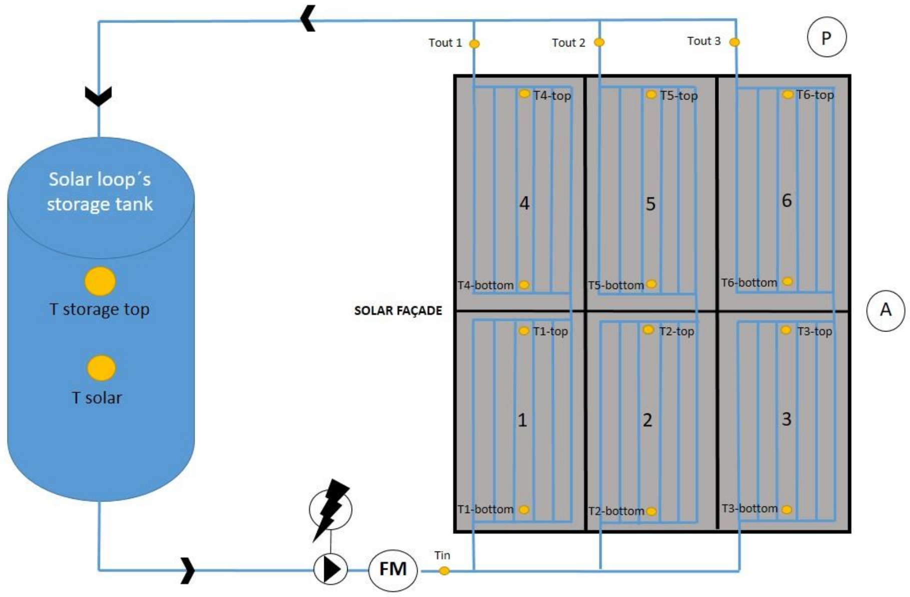

Figure 9: Diagram of the installation and its main components

The individual uncertainty of each specific parameter as expressed in Table 3 defined by the corresponding measurement device, represents an accumulated uncertainty in the main calculated parameters used for the study. The Root Sum Square (RSS) method [61, 74] was used for estimating the combined uncertainty in the calculated parameters.

$$u_{yo} = \sqrt{\left(\frac{\delta y}{\delta x_1}\, u_{x1}\right)^2 + \cdots + \left(\frac{\delta y}{\delta x_n}\, u_{xn}\right)^2} \tag{17}$$

Being u_y the overall uncertainty for each main parameter (y), and u_x the individual errors, of the measured parameters (x).

The temperature difference (T_{out}-T_{in}) is affected by the temperature input and output in the collector. This temperature difference combined with the mass flow influences the Energy output (Q) as in equation 2, while the energy, when divided by the irradiance (equation 21), represents the efficiency (η). The resulting uncertainties for the calculated parameters are 0.48% for the temperature difference, 7,83% for Q and 9.29% for η.

4.2 Experimental validation of the model

The first definition of the model is based on the specific design as constructed for the ASTF installed in the real building. From the set of 6 panels ($3m^2$ each) 2 panels connected in series as described in previous section, are considered first for the validation and parametric assessment. In a second verification all the 6 panels are considered. The parameters for the 2 panel battery are indicated in table 4.

Table 4. Initial configuration for the model

Parameter	**Material / Value**
Skin material	Steel (λ = 50 W/m^2K)
Skin thickness	0.7mm
Absorptivity	0.8
Panel dimensions	6m long / 1m wide / 82.1mm thick
Tube material	Nylon (λ = 0.2 W/m^2K)
Inner tube diameter / wall thickness	8mm / 2mm
Fluid	water
Spacing between parallel pipes	160 mm
Mass flow	8 l/min

Experimentally measured parameters I_{sol}, T_{amb}, T_{in}, V_w and $\dot{m}$, are used as inputs. Values recorded in 1-minute frequency were clustered in an hourly basis to smooth the transitory effects while the performance of the collector can be represented during different periods in the day.

T_{amb}, T_{in} and $\dot{m}$ are direct inputs to the model while the irradiation is transformed in a heat flux and the wind velocity is used to estimate the heat transfer coefficient (h_W).The three possible h_w correlations were calculated for one day (19th June 2017) concluding that the one by Wattmuff et Al. [68] has the lowest PMAE = 1.22% compared with the one for Test et Al. [70] 1.29% and for McAdams [69] 1.32%.

The model simulation provided the calculated values for the water outlet temperature and the absorber temperature over three consecutive days in June 2017. The solar loop was settled for a continuous flow throughout the whole period with no interruption, to observe the dynamic thermal effects.

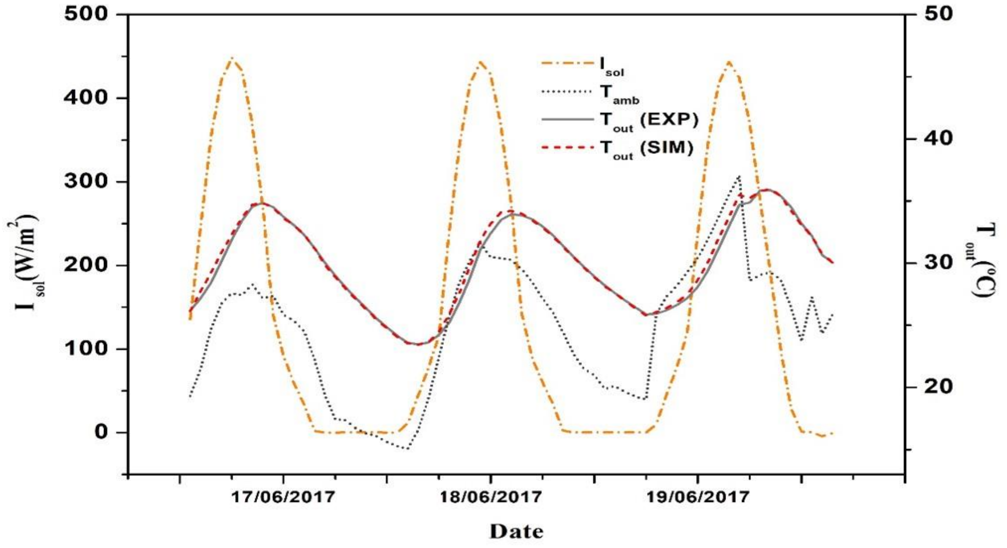

a)

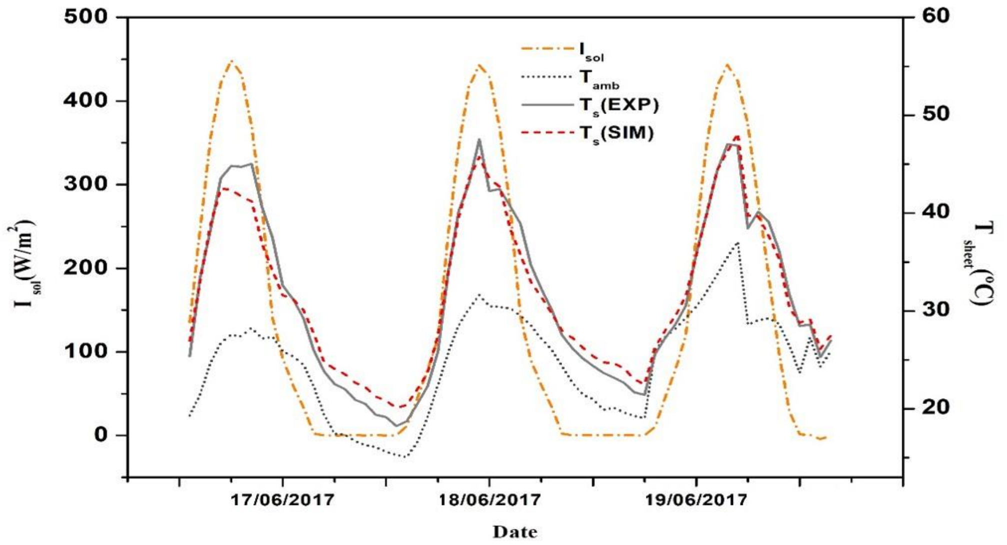

b)

Figure 10: Validation of the simulated results for T_{out} (a) and T_s (b) compared with experimental values for 17 to 19 of June in 2017.

The differences between real and simulated T_{out} during cooling at night showed a better match than during daytime heating (Figure 10 a). For T_s the effect is the opposite, in that the heating effect showed greater similarity between simulated and measured values (Figure 10 b). The variation between experimental and simulated values over the three days resulted in a PMAE of 1.08% for T_{out} and 4.2% for T_s.

One possible reason for the differences in skin temperatures is identified in the temperature distribution in the real case, compared with a continuous and regular temperature profile estimated by the model. In the real case, skin temperatures have an irregular distribution, mainly because of the contact points between the external and the internal skins and the pipes are not fully satisfactory. Although the sensors recorded a mean value of 34.58ºC at that moment, the thermographic image in Figure 11 qualitatively highlights significant differences in various zones of the façade surface.

Figure 11: Thermography of the active façade

As an additional verification, the output temperature was simulated for the complete set of 6 panels (18m^2 of active surface) increasing the mass flow rate up to 13.8 l/min. Figure 12 shows the differences between the simulated and the real values over one day in August when the PMAE was calculated at 1.43%.

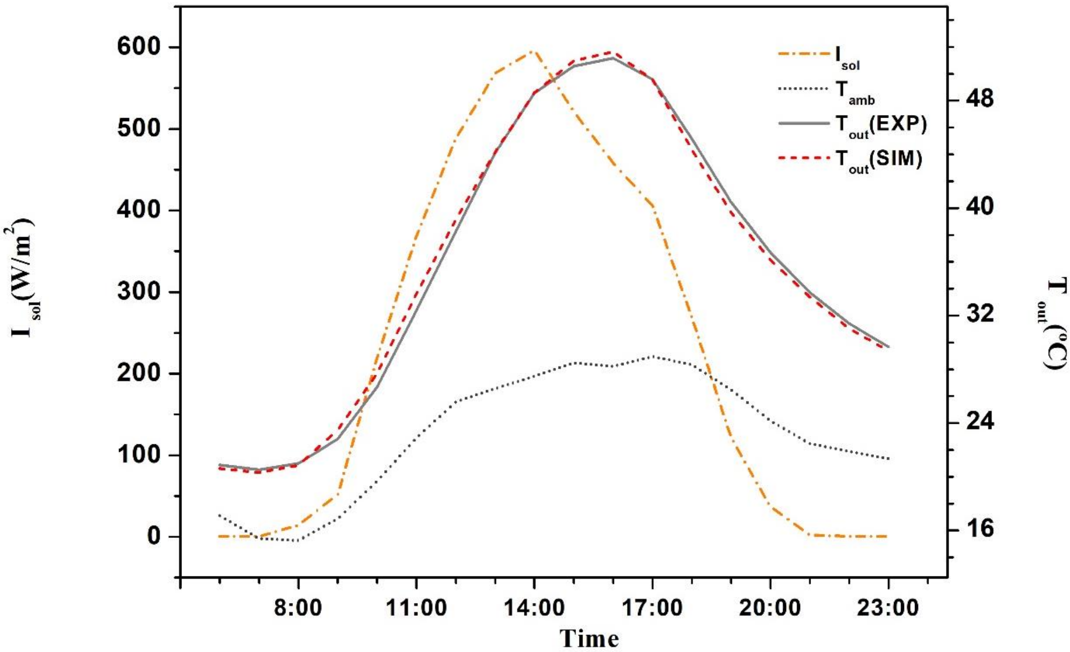

Figure 12: Second validation of the simulated results for T_{out} compared with experimental values for different panel surface and mass flow rate

5. Active façade design alternatives and performance assessment

5.1 Parametric Assessment

Having validated the CFD model, a parametric study was performed to evaluate alternatives to the specific design of each component of the active façade: the panel and the hydraulic circuit. The assessment was calculated with the external environmental conditions of a day in late spring (19^{th} June 2017). The reference system of $6m^2$ active surface, described in Table 4, provided an efficiency rate of 35.1% on that day.

5.1.1 Sandwich panel alternatives

Metallic sheets:

Conductivity is mainly associated with the type of material that is used to solve the two external layers. The third internal layer contributes nothing to the thermal performance of the collector. Although combinations are feasible, all the three sheets are assumed to be made of the same material.

The main interest relates to the external sheet that acts as the absorber. Conductivity is decisive, since it allows, on the one hand, the homogenization of the temperature of the entire surface and, on the other hand, it transfers heat from the absorber to the hydraulic circuit with greater efficiency.

Conductivity of the sheet and the amount of conductive material are beneficial, so sheet thickness of the sheets is also important. Thus, a plate with a high conductivity, sufficient thickness and a good contact surface between solids, will provide a good driving phenomenon between the absorber and the hydraulic circuit.

For the thickness, metal sheets in this applications are generally thinner (0.2 to 2.5 mm) than other materials such as concrete or polymers that usually require more material (5 – 50 mm) to configure continuous layers. For the thickness assessment, as the reference system is based on steel, the range of adopted values consider the parameters of that metal.

Figure 13-a shows the increased thermal conductivity of the external sheets, with a strong increase for metal sheets compared with non-metallic sheets, although a significant effect can be appreciated depending on the metal chosen. The extremes between the lowest conductive material (polymeric) and the highest conductive one (copper) represents an efficiency difference of 32%. A similar progression can be appreciated for the thickness (Figure 13-b) although values over 1mm represent a small improvement compared with the increase of the weight and material, directly influencing the cost of the system.

Absorber absorptivity:

Absorptivity depends on both the material and the type of finish or coating. Figure 13-c shows the effect of modifying absorptivity, demonstrating that it is one of the most influential parameters of daily efficiency with a difference of 31% for the range of values under consideration. As indicated in equation 3, the relation between λ and η is quite linear and the shape of the curve follows that progression.

Insulation material:

The main function of the insulation is the prevention of heat loss through the inner side of the panel. Polyurethane is commonly used in sandwich panels and is therefore used as the reference material. Alternative materials considered to have insulation properties (<0.5 W/m^2K) are also calculated. In addition, an alternative without any insulation is estimated to consider the consequences of a simplified system.

In the assessment of the insulation material, the adiabatic condition established for the back sheet (sheet nº3 in figure 2) no longer applied and the convective effect for the air cavity was set to 5 W/m^2K. In general terms, the effect of insulation on efficiency was less significant (Figure 13-d and 13-e) rather than for the case of the metal sheets, but the interest of having at least a minimum level of a material (10mm) with insulating properties has an important effect.

5.1.1 Alternatives for the hydraulic circuit

Piping system:

Pipe spacing will determine the number of parallel pipes per square meter in the collector. A higher density implies a higher exchange surface, but also an increase in system costs and complexity. Figure 13-f shows a small decrease of nearly 1% for each additional 40 mm in pipe spacing.

The conductivity of the pipes was equivalent to the conductivity of the external sheet, thus available materials are also similar. As a consequence, the impact of changes to conductivity in daily efficiency provided a similar progression (Figure 13-g) for both highly conductive metals and plastics with lower conductivities. If plastic rather than metal piping is used, there is a very significant efficiency difference of 15%. In this case, there is no great difference in the specific metal that is employed (differences of 0.1% in the efficiency), so if a metallic system is adopted, the cost factor could determine the specific metal for the piping system.

The inner diameter and the wall thickness of the pipe are parameters defined by the type of material and conventional piping products that are usually available for such hydronic applications. The inner diameter is the main parameter considered in the calculation. It represents an increase in efficiency together with the increased diameter (Figure 13-h) for a maximum performance level at 12mm, although 8mm and 10mm cases have quite similar responses. Efficiency decreases with a smooth slope for diameters higher than 12mm.

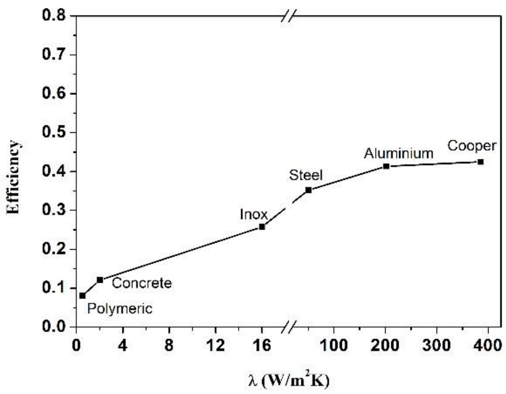

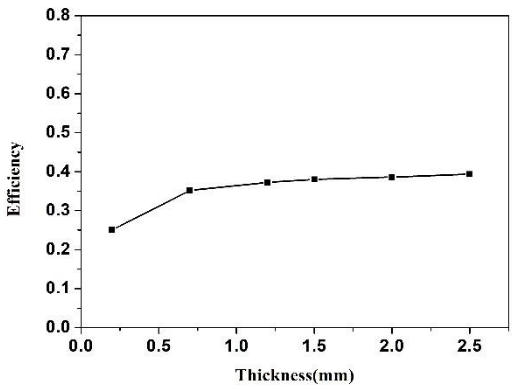

a) b)

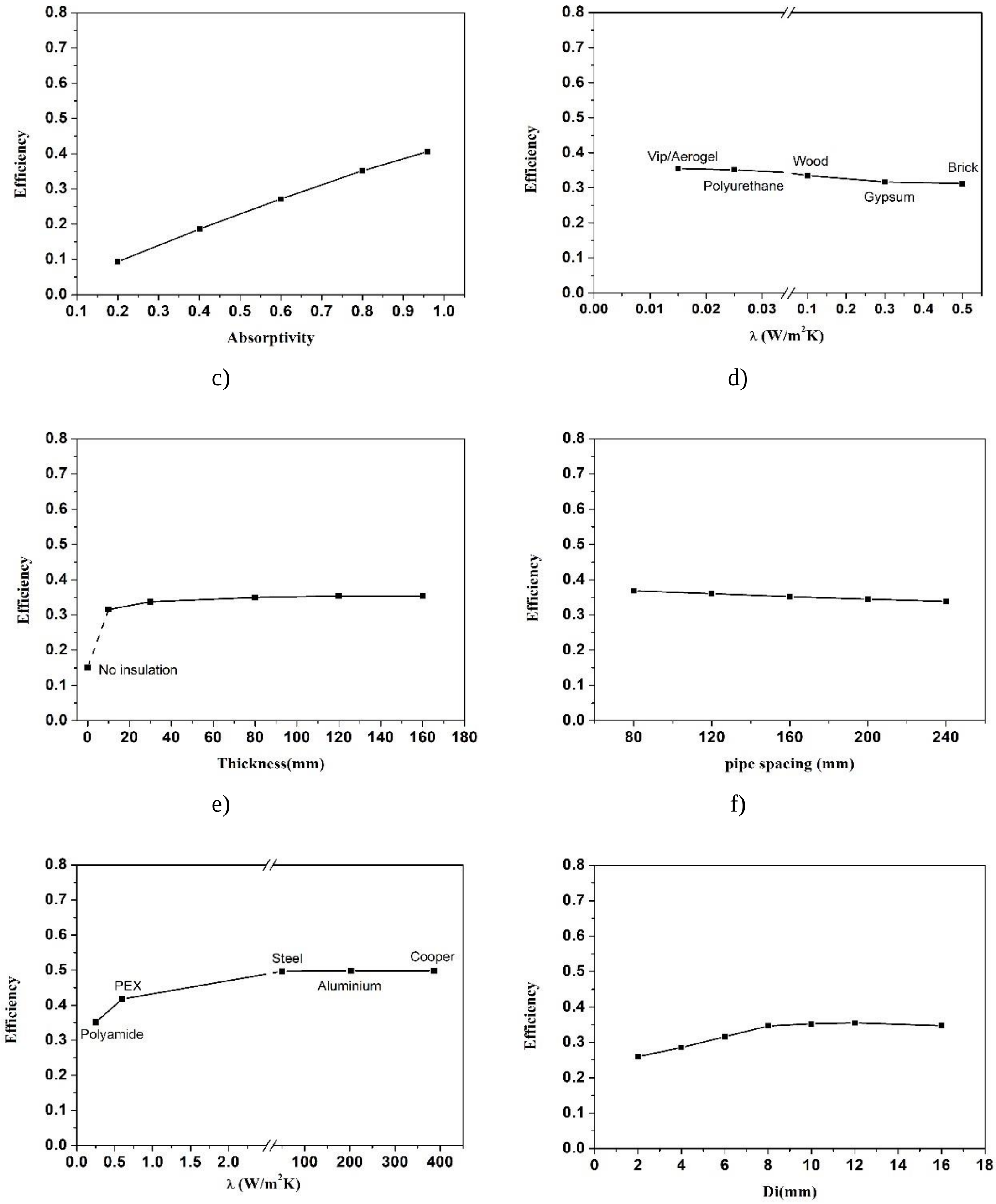

g) h)

Figure 13 Parametric assessments for the ASTF. Variation of the efficiency for alternatives in: a) External sheet conductivity; b) Sheet thickness; c) Absorptivity; d) Insulation conductivity; e) Insulation thickness; f) Pipe spacing; g) Pipe conductivity; and, h) Inner pipe diameter.

<u>Mass Flow and panel length</u>

The minimum flow rate was limited to 0.13 kg/s per m^2, regulated with a circulating pump in the real case. Different flow alternatives are considered in the study, ranging from 0.01 kg/s to 0.2 kg/s based on the bibliography [31]. Figure 14 (a) shows the variation of outlet temperature and daily efficiency depending on the mass flow rate. The increase in the mass flow also implies increased efficiency, but a lower output temperature.

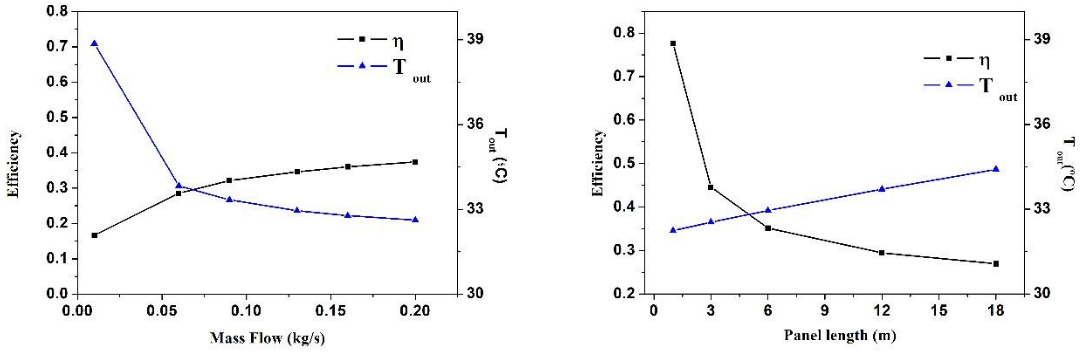

a) b)

Figure 14: Efficiency and Outlet temperature change for variations in the mass flow rate (a) and panel length (b).

The panel length is similar due to the equivalent flow relation, as described in section 4 (Figure 7). The length is of special relevance when defining active façades on the vertical axis where values multiple of 3 m. are typically considered between floor levels. It is a central constraint for these façade applications where values under 3 meters generally represent greater difficulties for integration.

5.2 Performance of the Active Façade under real working conditions

A panel production analysis was also performed between March and August 2017, to conclude the study. In this way, the potential of the active façade was calculated and the potential energetic production of the system was quantified. The daily efficiency for solar yields of some significance ranged between 4 – 36% with a mean daily yield of 0.326 kWh/m^2 collected over that 6-month period.

Moreover, the performance of the system was calculated with a regression analysis carried out using the data collected over one complete month during the overall campaign. The efficiency factors of the installed system were calculated for four different wind speeds, by means of a linear regression, as indicated in Table 5 and Figure 15, respectively, where the effect of the wind can be clearly appreciated.

Table 5 Efficiency parameters of the Active Façade as a result of the regression analysis

Wind Speed	**Slope ($F_R\ U_L$)**	**Intercept ($F_R\ a$)**	**Adj. R^2**
$0 < V_w < 1$	-4.851	0.47	0.96
$1 < V_w < 2$	-6.886	0.44	0.96
$2 < V_w < 3$	-7.391	0.39	0.97
$3 < V_w < 4$	-7.501	0.34	0.96

Compared with the results for different systems, as presented in Table 1, the system installed and analyzed in the present study has lower efficiencies in general, but it also has a significantly (up to 6 times) higher total active surface than those other solutions, which has an effect on the final performance of the solution [45].

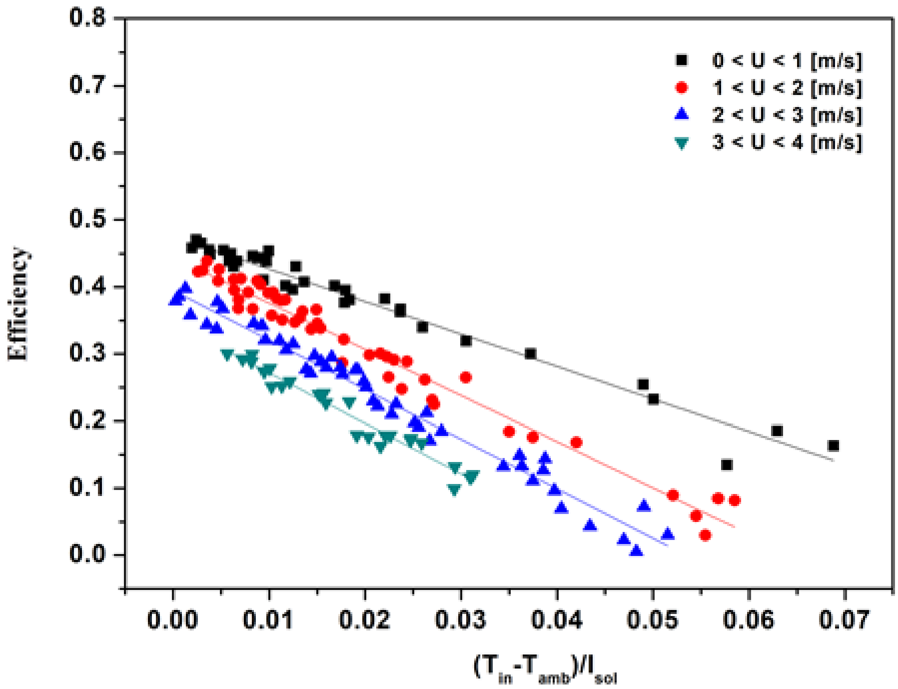

Figure 15: Efficiency curve regression for different wind velocities

6. Discussion of results

The results of all the simulations are presented in Figure 16. The variation of each independent parameter in relation to a base case system (35.1% efficiency) and its effect is described. The potential of each parameter can be appreciated resulting in maximum and minimum values in the daily efficiency of the system.

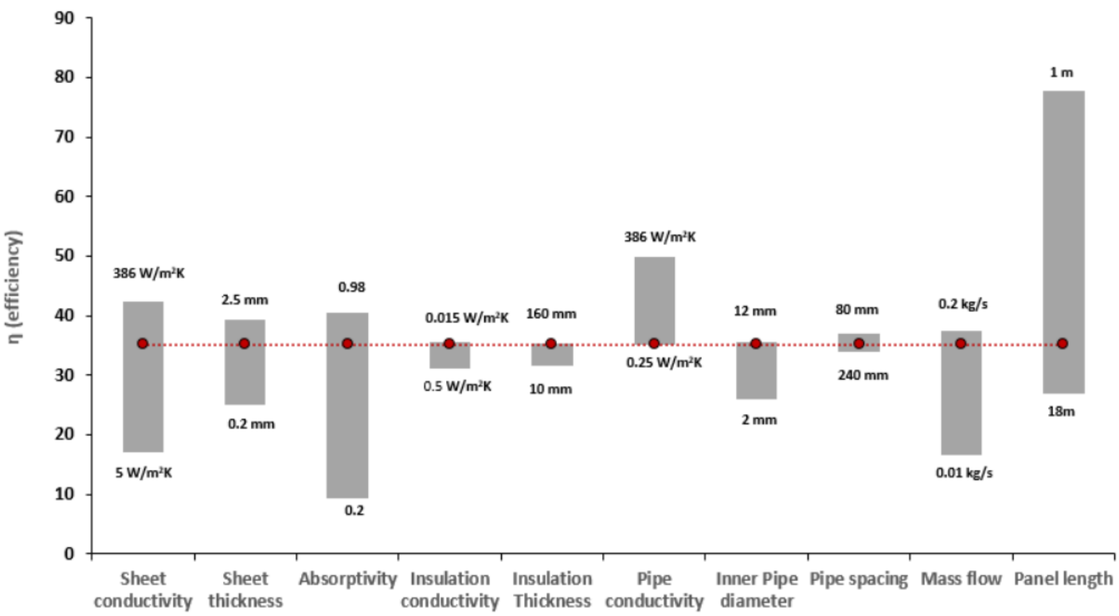

Figure 16: Results of the parametric study representing the maximum and minimum achievable efficiencies when one single parameter is modified

Parameters with strong effects on efficiency, starting with those with the highest variability are the panel length, absorptivity, sheet conductivity, mass flow, sheet thickness, pipe conductivity, and inner diameter. Besides, variations in pipe spacing, insulation thickness, and insulation conductivity have a limited influence and are not critical for the design.
Reviewing the real system and the model described in Table 4, it can be concluded that the design was in general terms within the upper range of almost all the parameters except in the case of panel length and pipe conductivity. Nevertheless, some other parameters still show room for improvement and different combinations to improve the efficiency are feasible.

If three of the most influential parameters are modified together to achieve a better solution, by switching the panel length to 3m, by switching the pipe conductivity to copper, and by increasing the absorptivity of the absorber to 0.98, a daily efficiency of 66% is estimated, achieving a combined effect rather than through independent modifications. Another alternative was in the form of a 6 m panel with copper pipes and a copper absorber that also achieved a daily efficiency of 66%. In this second calculation, Figure 17 shows the differences between the reference case and the improved one in the temperature difference (T_{out}-T_{in}) for the same input temperature (T_{in}) during the benchmark day.

As a result of the overall analysis, it can be concluded that the impact of the parameters on system efficiency is highly significant. If properly selected, those parameters can lead to higher efficiencies as well as to higher output temperatures resulting in higher solar production levels.

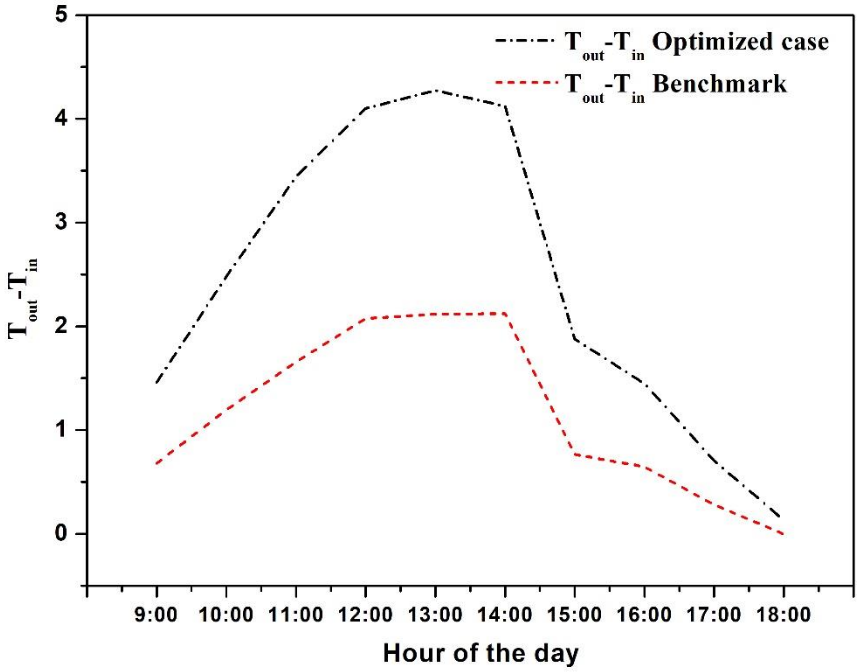

Figure 17: Simulated values for the thermal difference (T_{out}-T_{in}) comparing the benchmark design with an optimized case.

7. Conclusions

In the present study, an active façade application integrating an unglazed collector inside a metallic sandwich panel has been tested. By means of a methodology based on a theoretical model, a bespoke CFD model has been developed and validated, permitting a parametric assessment for the evaluation of design alternatives. The validation process was done by recording data on a set of 6 ASTF prototype panels (3m^2 each) installed at Tecnalia's Kubik® experimental building in Derio (Spain), over an extensive monitoring campaign in 2017.

The analysis of the production for that period has concluded in a mean 0.326kWh/m^2 daily monitored yield. A relevant effect of the wind on lowering the efficiencies has also been demonstrated, resulting in a 0.34 – 0.47 efficiency range (FR α) and a 4.851 – 7.501 energy loss factor range (FR UL) for different wind speeds.

The results of the assessment have highlighted the relevance of some parameters on the final thermal performance of the ASTF. The system's length, its absorptivity and the materials employed are identified as key design parameters. Metals with high absorptivity in the absorber ($\lambda > 50$ W/m^{2}K & $\alpha > 0.9$) turns out to be beneficial for this application. For the hydraulic circuit, as for the absorber, the use of metals provides a direct impact on increased efficiency. For the inner diameter of the pipes the optimum value for the present application is calculated at 12mm.

In parallel, the lesser relevance of some other parameter has been demonstrated. The type and thickness of insulation is not a critical factor, so far as there is at least a minimum insulation (10mm thick and < 0.04 W/m^{2}K). For the hydraulic circuit the density of pipes per m^2 has also a low significance for the ranges evaluated.

As a general conclusion of the study, combining calculated and measured results, the need for proper comprehension of these active systems and their impact is clear. Looking further for specific applications additional research will still be needed, to evaluate combinations of active components integrated in the heating production systems and to assess their combined performance, as well as potential synergetic approaches

Nomenclature

Q	Heat transferred to the thermal fluid	kJ
A_c	Collector area	m^2
S	Pipe section	m^2
$\dot{m}$	Mass flow rate	kg/s
t_s	Sheet thickness	m
F_R	Heat removal factor	(-)
U_L	Heat transfer coefficient	$W/(m^2K)$
$F_R U_L$	Heat Loss Factor	$W/(m^2K)$
C_w	Specific heat capacity of water	kJ/kg K
C_L	Variable parameter (equations 6 and 7)	1/m
T_{out}	Outlet water temperature	ºC
T_{in}	Inlet water temperature	ºC
T_{amb}	Ambient temperature	ºC
T_s	External skin-surface temperature	ºC
T_{sky}	Sky temperature	ºC
T_p	Pipe wall temperature	ºC
T_f	Fluid temperature	ºC
I_{sol}	Solar irradiation	$W/(m^2)$
F'	Collector efficiency factor	(-)
F	Standard fin efficiency for straight fins	(-)
D_i	Hydraulic diameter of each pipe	m
W	Pipe Spacing	m
h_f	Convective heat transfer coefficient between fluid and pipe wall	$W/(m^2K)$
q_i	Heat flux absorbed by the solar collector	kW/m^2
q_{rad}	Heat flux lost by radiation	kW/m^2
$q_{f,c}$	Heat flux lost by forced convection	kW/m^2
$q_{n,c}$	Heat flux lost by natural convection	kW/m^2
q_f	Heat flux absorbed by the fluid	kW/m^2
h_W	Convective heat transfer coefficient between external skin and air	$W/(m^2K)$
Pr	Prandlt number	(-)
Re	Reynolds number	(-)
ν_k	Kinematic viscosity	m^2/s
μ	Viscosity	Kg/(m s)
V_W	Wind speed	m/s
V	Inlet water velocity	m/s
L	Pipe length	m

Greek symbols

λ	Conductivity	$W/(m^2K)$
λ_s	External conductivity of skin	$W/(m^2K)$
η	Efficiency	%

α	Absorptivity	(-)
ε	Emissivity	(-)
σ	Stefan Boltzman constant	$W/(m^2K^4)$
τ	Hydraulic residence time	s

Acronyms

NZEB	Nearly Zero Energy Buildings
RES	Renewable Energy Sources
SF	Solar Façade
ASTF	Active Solar Thermal Façade
BISTS	Building Integrated Solar Thermal Systems
RANS	Reynolds-averaged Navier-Stokes
SIMPLE	Semi-Implicit Method for Pressure Linked Equations
PMAE	Predicted Mean Absolute Error

Acknowledgements

The authors are grateful to the Basque Government for funding this research through projects IT781-13 and IT1314-19 and to all those involved in the different stages for their guidance and invaluable help.

The authors would also like to thank all those companies and researchers participating in the BASSE project for their strong involvement during that research. Results from BASSE project have inspired present research. The BASSE project received funding from the European Union, RFCS Program, Research Fund for Coal and Steel project Building Active Steel Skin (BASSE, Grant Agreement no RFSR-CT-2013-00026).

References

[1] Commission Recommendation (EU) 2016/1318, of 29 July 2016 on guidelines for the promotion of nearly zero-energy buildings and best practices to ensure that, by 2020, all new buildings are nearly zero-energy buildings. https://eur-lex.europa.eu/legal-content/EN/TXT/?uri=CELEX%3A32016H1318 (Last accessed 8 February 2019)

[2] European Commission. (EU) Building Stock Observatory. Directorate-General for Energy, (2019) https://ec.europa.eu/energy/en/eubuildings. (Last accessed 8 February 2019)

[3] IEA. International Energy Agency. Transition to Sustainable Buildings. Strategies and Opportunities to 2050. (2013)

[4] T.S. Ge, R.Z. Wang, Z.Y. Xu, Q.W. Pan, S. Du, X.M. Chen, T. Ma, X.N. Wu, X.L. Sun, J.F. Chen, Solar heating and cooling: Present and future development, Renew. Energy. 126 (2018) 1126–1140. doi:10.1016/J.RENENE.2017.06.081.

[5] R. O'Hegarty, O. Kinnane, S.J. McCormack, Review and analysis of solar thermal facades, Sol. Energy. 135 (2016) 408–422. doi:10.1016/J.SOLENER.2016.06.006.

[6] A. Giovanardi, A. Passera, F. Zottele, R. Lollini, Integrated solar thermal façade system for building retrofit, Sol. Energy. 122 (2015) 1100–1116. doi:10.1016/J.SOLENER.2015.10.034.

[7] X. Zhang, J. Shen, Y. Lu, W. He, P. Xu, X. Zhao, Z. Qiu, Z. Zhu, J. Zhou, X. Dong, Active Solar Thermal Facades (ASTFs): From concept, application to research questions, Renew. Sustain. Energy Rev. 50 (2015) 32–63. doi:10.1016/J.RSER.2015.04.108.

[8] C.-M. Lai, S. Hokoi, Solar façades: A review, Build. Environ. 91 (2015) 152–165. doi:10.1016/J.BUILDENV.2015.01.007.

[9] G. Quesada, D. Rousse, Y. Dutil, M. Badache, S. Hallé, A comprehensive review of solar facades. Opaque solar facades, Renew. Sustain. Energy Rev. 16 (2012) 2820–2832. doi:10.1016/J.RSER.2012.01.078.

[10] G. Quesada, D. Rousse, Y. Dutil, M. Badache, S. Hallé, A comprehensive review of solar facades. Transparent and translucent solar facades, Renew. Sustain. Energy Rev. 16 (2012) 2643–2651. doi:10.1016/J.RSER.2012.02.059.

[11] I. Visa, M. Moldovan, M. Comsit, M. Neagoe, A. Duta, Facades Integrated Solar-thermal Collectors - Challenges and Solutions. Energy Procedia 112 (2017). 176–185. https://doi.org/10.1016/j.egypro.2017.03.1080.

[12] COST Action TU1403. Adaptive Facades Network. http://tu1403.eu/ (Last accessed 8 February 2019)

[13] Z. Nagy, B. Svetozarevic, P. Jayathissa, M. Begle, J. Hofer, G. Lydon, A. Willmann, A. Schlueter, The Adaptive Solar Facade: From concept to prototypes, Front. Archit. Res. 5 (2016) 143–156. doi:10.1016/J.FOAR.2016.03.002.

[14] M. C. Munari Probst, C. Roecker, Towards an improved architectural quality of building integrated solar thermal systems (BIST). Sol. Energy, 81 (2007) 1104–1116. https://doi.org/10.1016/j.solener.2007.02.009.

[15] C. Lamnatou, J.D. Mondol, D. Chemisana, C. Maurer, Modelling and simulation of Building-Integrated solar thermal systems: Behaviour of the coupled building / system configuration. Renew. Sustain. Energy Rev, 48 (2015) 178–191. https://doi.org/10.1016/j.rser.2015.03.075.

[16] S.A. Kalogirou, Solar thermal collectors and applications, Prog. Energy Combust. Sci. 30 (2004) 231–295. doi:10.1016/J.PECS.2004.02.001.

[17] M. C. Munari Probst, & C. Roecker, (2011) Architectural Integration and Design of Solar Thermal Systems. 1st Edition. EPFL Press. Lausanne, Switzerland. ISBN-13: 978-0415667913.

[18] S. Kalogirou, Y. Tripanagnostopoulos, M. Souliotis, Performance of solar systems employing collectors with colored absorber, Energy Build. 37 (2005) 824–835. doi:10.1016/J.ENBUILD.2004.10.011

[19] T.N. Anderson, M. Duke, J.K. Carson, The effect of colour on the thermal performance of building integrated solar collectors. Sol. Energy Mater. Sol. Cells, 94 nº2 (2010) 350–354. https://doi.org/10.1016/j.solmat.2009.10.012.

[20] IEA, SHC Task 39. Polymeric Materials for Solar Thermal Applications. http://task39.iea-shc.org (Last accessed 8 February 2019)

[21] D. Missirlis, G. Martinopoulos, G. Tsilingiridis, K. Yakinthos, N. Kyriakis, Investigation of the heat transfer behaviour of a polymer solar collector for different manifold configurations, Renew. Energy. 68 (2014) 715–723. doi:10.1016/J.RENENE.2014.03.008

[22] R. O'Hegarty, O. Kinnane, S.J. McCormack, Parametric investigation of concrete solar collectors for façade integration, Sol. Energy. 153 (2017) 396–413. doi:10.1016/J.SOLENER.2017.05.092.

[23] A. Sable, Experimental and economic analysis of concrete absorber collector solar water heater with use of dimpled tube, Resour. Technol. 3 (2017) 483–490. doi:10.1016/J.REFFIT.2017.06.001.

[24] Y. Yang, Q. Wang, D. Xiu, Z. Zhao, Q. Sun, A building integrated solar collector: All-ceramic solar collector, Energy Build. 62 (2013) 15–17. doi:10.1016/J.ENBUILD.2013.03.002.

[25] X. Sun, X. Sun, X. Li, Z. Wang, J. He, B. Wang, Performance and building integration of all-ceramic solar collectors. Energy Build., 75 (2014) 176–180. https://doi.org/10.1016/j.enbuild.2014.01.045.

[26] A. Pugsley, A. Zacharopoulos, M. Smyth, J. Mondol, Performance evaluation of the senergy polycarbonate and asphalt carbon nanotube solar water heating collectors for building integration, Renew. Energy. (2017). doi:10.1016/J.RENENE.2017.10.082.

[27] B. Nábìlek, E. Kiran, F. Türksoy, A. Yazar, Performance of an unglazed textile-plastic solar absorber, Renew. Energy. 16 (1999) 635–638. doi:10.1016/S0960-1481(98)00241-9.

[28] W. Weiss, & M. Spörk-Dür, (2018). Solar Heat Worldwide. 2018 Edition. Global Market Development and Trends in 2017. Detailed Market Figures 2016. https://www.iea-shc.org/Data/Sites/1/publications/Solar-Heat-Worldwide-2018.pdf (Last accessed 8 February 2019)

[29] B. Bokor, H. Akhan, D. Eryener, L. Kajtár, Theoretical and experimental analysis on the passive cooling effect of transpired solar collectors, Energy Build. 156 (2017) 109–120. doi:10.1016/J.ENBUILD.2017.09.063.

[30] X. Wang, B. Lei, H. Bi, T. Yu, A simplified method for evaluating thermal performance of unglazed transpired solar collectors under steady state, Appl. Therm. Eng. 117 (2017) 185–192. doi:10.1016/J.APPLTHERMALENG.2017.01.053.

[31] C. Maurer, C. Cappel, T.E. Kuhn, Progress in building-integrated solar thermal systems, Sol. Energy. 154 (2017) 158–186. doi:10.1016/J.SOLENER.2017.05.065.

[32] M.S. Buker, S.B. Riffat, Building integrated solar thermal collectors – A review, Renew. Sustain. Energy Rev. 51 (2015) 327–346. doi:10.1016/J.RSER.2015.06.009.

[33] T. Matuska, B. Sourek, Façade solar collectors. Sol. Energy, 80 (2006) 1443–1452. https://doi.org/10.1016/j.solener.2006.04.006.

[34] A. Buonomano, C. Forzano, S.A. Kalogirou, A. Palombo, Building-façade integrated solar thermal collectors: Energy-economic performance and indoor comfort simulation model of a water based prototype for heating, cooling, and DHW production, Renew. Energy. (2018). doi:10.1016/J.RENENE.2018.01.059.

[35] L. Aelenei, M. Smyth, W. Platzer, B. Norton, D. Kennedy, S. Kalogirou, C. Maurer, Solar Thermal Systems – Towards a Systematic Characterization of Building Integration, Energy Procedia. 91 (2016) 897–906. doi:10.1016/J.EGYPRO.2016.06.256.

[36] P. Elguezabal, B. Arregi, (2018). An analysis of the potential of envelope-integrated solar heating and cooling technologies for reducing energy consumption in European climates. Journal of Facade Design and Engineering. Vol. 6, nº 2 (2018), 085-094. https://doi.org/10.7480/jfde.2018.2.2102.

[37] M. Wall, M. C. Munari Probst, C. Roecker, M. C. Dubois, M. Horvat, O. B. Jørgensen, K. Kappel, Achieving solar energy in architecture - IEA SHC Task 41. Energy Procedia, 30 (2012) 1250–1260. https://doi.org/10.1016/j.egypro.2012.11.138.

[38] A. Gagliano, S. Aneli, F. Nocera, Analysis of the performance of a building solar thermal facade (BSTF) for domestic hot water production. Renew. Energy, 142 (2019) 511–526. https://doi.org/10.1016/j.renene.2019.04.102.

[39] C. Lamnatou, G. Notton, D. Chemisana, C. Cristofari, Life cycle analysis of a building-integrated solar thermal collector, based on embodied energy and embodied carbon methodologies. Energy Build., 84 (2014) 378–387. https://doi.org/10.1016/j.enbuild.2014.08.011.

[41] F. Motte, G. Notton, C. Cristofari, J. Canaletti, Design and modelling of a new patented thermal solar collector with high building integration. Appl. Energy, 102 (2013) 631–639. https://doi.org/10.1016/j.apenergy.2012.08.012.

[42] D. Rodríguez-Sánchez, J.F. Belmonte, M.A. Izquierdo-Barrientos, A. E. Molina, G Rosengarten, Solar energy captured by a curved collector designed for architectural integration. Appl. Energy 116 (2014) 66–75. https://doi.org/10.1016/j.apenergy.2013.10.059.

[43] A. K. Furundzic, V. Kosoric, K. Golic, Potential for reduction of CO2 emissions by integration of solar water heating systems on student dormitories through building refurbishment. Sustain. Cities Society, 2 nº1 (2012) 50–62. https://doi.org/10.1016/j.scs.2011.10.005.

[44] C. Cappel, W. Streicher, F. Lichtblau, C. Maurer, Barriers to the market penetration of façade-integrated solar thermal systems. Energy Procedia 48 (2014) 1336–1344. https://doi.org/10.1016/j.egypro.2014.02.151.

[45] S. Medved, C. Arkar, B. Černe, A large-panel unglazed roof-integrated liquid solar collector––energy and economic evaluation, Sol. Energy. 75 (2003) 455–467. doi:10.1016/J.SOLENER.2003.09.009.

[46] Energie Solaire SA. http://www.energie-solaire.com. (Last accessed 8 February 2019)

[47] Solabs, 2006. SOLABS. Development of unglazed solar absorbers (resorting to coloured selective coatings on steel material) for building facades, and integration into heating systems (solabs) – Project reference: ENK6-CT-2002-00679. Retrieved from http://cordis.europa.eu/project/rcn/67210_en.html. (Last accessed 8 February 2019)

[48] P. Bonhôte, Y. Eperon, P. Renaud, Unglazed coloured solar absorbers on façade: Modelling and performance evaluation, Sol. Energy. 83 (2009) 799–811. doi:10.1016/J.SOLENER.2008.11.014.

[49] Triple Solar BV. https://www.triplesolar.eu/home/ (Last accessed 8 February 2019)

[50] BATISOL Project, INEF4, Institut pour la Transition Enérgétique, www.inef4.com (Last accessed 8 February 2019)

[51] Inroof Solar. https://www.inroof.solar/ (Last accessed 8 February 2019)

[52] S. Boudjabeur et Al. Building Active Steel Skin. (BASSE). Grant Agreement nº: RFSR-CT-2013 - 00026. Final Report. ISBN 978-92-79-94133-7. ISSN 1831-9424. doi: 10.2777/767032. Retrieved from https://publications.europa.eu/en/web/general-publications/publications (Last accessed 26 June 2019)

[53] P. Elguezabal, R. Garay, K. Martin, Experimentation under real performing conditions of a highly integrable unglazed solar collector into a building façade. Energy Procedia. Vol. 122 (2017), 775-780. doi. https://doi.org/10.1016/j.egypro.2017.07.395

[54] J. Duffie, W. Beckmann, Solar Engineering of Thermal Processes, fourth Ed., Hoboken, New Jersey, 2013.

[55] 10002035 Certification. INroof.solar Nor'eastern. Solar Rating and Certification Corporation (SRCC). http://www.solar-rating.org/ (Last accessed 8 February 2019)

[56] C1209 Test Collector Factsheet. Energie Solaire Kollektor AS. SPF Institute for Solar Technology http://www.spf.ch (Last accessed 8 February 2019)

[57] TECU® Solar System Factsheet. http://www.kme.com (Last accessed 8 February 2019)

[58] QUICK STEP® SolarThermie Factsheet. www.rheinzink.de (Last accessed 8 February 2019)

[59] R. Garay-Martinez, B. Arregi-Goikolea, P. Bonnami, S. Raji, J. Lopez, Concept, development and thermal characterization of an unglazed solar thermal collector for façade integration. DYNA, 92 nº4 (2017). 466-472. DOI: http://dx.doi.org/10.6036/8108

[60] M. Walsh, & W. Lin, A Parametric Study on the Thermal Performance of Unglazed Solar Water Collectors with Their Colorbond Steel Absorber Plates Also Used as Roofs. International Journal of Green Energy, 12 (2015), 1309–1322. https://doi.org/10.1080/15435075.2013.858045

[61] R. O'Hegarty, O. Kinnane, S.J. McCormack, Concrete solar collectors for façade integration: An experimental and numerical investigation, Appl. Energy. 206 (2017) 1040–1061. doi:10.1016/J.APENERGY.2017.08.239.

[62] D.G. Gunjo, P. Mahanta, P.S. Robi, CFD and experimental investigation of flat plate solar water heating system under steady state condition, Renew. Energy. 106 (2017) 24–36. doi:10.1016/J.RENENE.2016.12.041.

[63] J. Allan, Z. Dehouche, S. Stankovice, & A. Harries, Computational Fluid Dynamics Simulation and Experimental Study of Key Design Parameters of Solar Thermal Collectors. Journal of Solar Energy Engineering, 139 nº5 (2017) 051001-1. https://doi.org/10.1115/1.4037090

[64] H. Schober, D. Brandl, M. Zellinger, T. Mach, O. Englhardt, Hybrid Element Façade - Thermal Engineering and Related Structural Evaluation of a Solar Activated Integral Panel. Advanced Building Skins 2012 - TU Graz, Graz, Austria. Conference Proceedings (2015) 89 – 101. ISBN: 978-3-85125-397-9. Retrieved from http://lamp.tugraz.at/~karl/verlagspdf/advanced-building-skins.pdf (Last accessed 8 February 2019)

[65] L.P.M. Colombo, C.M. Joppolo, L. Molinaroli, E. Rovelli, An Approximate Analytical Approach to Steady State Simulation of Unglazed Solar Collectors, Energy Procedia. 48 (2014) 28–36. doi:10.1016/J.EGYPRO.2014.02.005.

[66] D. Brandl, H. Schober, C. Hochenauer, Analysis of Heating Effects and Deformations for a STAF Panel with a Coupled CFD and FEM Simulation Method. Journal of Facade Design & Engineering, 6 nº3 (2018) 116–131. https://doi.org/10.7480/jfde.2018.3.2567

[67] S. Kumar, S.C. Mullick, Wind heat transfer coefficient in solar collectors in outdoor conditions, Sol. Energy. 84 (2010) 956–963. doi:10.1016/J.SOLENER.2010.03.003.

[68] J.H. Wattmuff, W.W.S. Charters, D. Proctor, Solar and wind induced external coefficients for solar collectors. Internationale Révue d'Heliotechnique 2, (1977) 56

[69] W.H. McAdams, Heat Transmission, third ed., Tokyo, Japan, 1954.

[70] F.L. Test, R.C.L. Lessman, A. Johary, Heat transfer during wind flow over rectangular bodies in natural environment. Transactions of the ASME Journal of Heat Transfer 103 (1981) 262–267

[71] ANSYS Inc., Ansys Fluent User's Guide, Release 18.0. 2017

[72] L.M. Ayompe, A. Duffy, S.J. McCormack, M. Conlon, Validated TRNSYS model for forced circulation solar water heating systems with flat plate and heat pipe evacuated tube collectors, Appl. Therm. Eng. 31 (2011) 1536–1542. doi:10.1016/J.APPLTHERMALENG.2011.01.046.

[73] J.A. Chica, I. Apraiz, P. Elguezabal, M. O. Rrips, V. Sánchez, B. Tellado, Kubik: Open building approach for the construction of an unique experimental facility aimed to improve energy efficiency in buildings. Open House International, 36 nº1 (2011) 63–72.

[74] J. Taylor, An Introduction to Error Analysis, the Study of Uncertainties in Physical Measurements, 2nd Edition, University Science Books, Sausalito, California, 1997.